

1    **Autophagy Suppresses CCL2 to Preserve Appetite and Prevent Lethal Cachexia**

2

3    Maria Ibrahim<sup>1,2</sup>, Maria Gomez-Jenkins<sup>1,2</sup>, Adina Scheinfeld<sup>2</sup>, Zhengqiao Zhao<sup>3</sup> Eduardo Cararo  
4    Lopes<sup>1</sup>, Akshada Sawant<sup>1,2</sup>, Zhixian Hu<sup>1,2</sup>, Aditya Dharani<sup>1</sup>, Michael Sun<sup>1</sup>, Sarah Siddiqui<sup>1</sup>,  
5    Emily T. Mirek<sup>4</sup>, Johan Abram-Saliba<sup>5</sup>, Edmund C. Lattime,<sup>1,6</sup> Xiaoyang Su<sup>1,6</sup>, Tobias  
6    Janowitz<sup>7</sup>, Marcus D. Goncalves<sup>8</sup>, Steven M. Dunn<sup>5</sup>, Yuri Pritykin<sup>2,3,9</sup>, Tracy G. Anthony<sup>1,2,4</sup>,  
7    Joshua D. Rabinowitz<sup>2</sup>, Eileen White<sup>1,2\*</sup>

8        1. Rutgers Cancer Institute, Rutgers University, New Brunswick, NJ 08903, USA

9        2. Ludwig Princeton Branch, Ludwig Institute for Cancer Research, Princeton University,  
10      Princeton, NJ 08544, USA

11      3. Lewis-Sigler Institute for Integrative Genomics, Princeton University, Princeton, NJ  
12      08540, USA

13      4. Department of Nutritional Sciences, Rutgers School of Environmental and Biological  
14      Sciences, Rutgers University, New Brunswick, NJ 08901, USA

15      5. LAbCore Immunoglobulin Discovery Platform, Department of Oncology, Ludwig  
16      Institute for Cancer Research-Lausanne, University Hospital and University of Lausanne,  
17      1066, Epalinges, Switzerland

18      6. Department of Medicine, Rutgers Robert Wood Johnson Medical School, New  
19      Brunswick, NJ 08901, USA

20      7. Cold Spring Harbor Laboratory, Cold Spring Harbor, NY 11724, USA; Northwell Health  
21      Cancer Institute, Northwell Health, New Hyde Park, NY 11042, USA

22      8. Departments of Medicine and Radiation Oncology, New York University, Grossman  
23      School of Medicine, Laura and Isaac Perlmutter Cancer Center, New York, NY 10016,  
24      USA

25      9. Department of Computer Science, Princeton University, Princeton, NJ 08540, USA

26      \*Corresponding author:

27      Eileen White, [epwhite@cinj.rutgers.edu](mailto:epwhite@cinj.rutgers.edu)

28

- 29 Key points of paper:
- 30 1) Autophagy-deficient mice have reduced food intake, systemic inflammation, and cachexia
- 31 2) CCL2, but not GDF15 or CXCL10, induces lethal cachexia caused by autophagy defect
- 32 3) Autophagy-deficient mice have CCL2-dependent destruction of appetite-promoting neurons
- 33 in the hypothalamus
- 34 4) Leptin deficiency restores appetite and rescues lethal cachexia in autophagy-deficient mice
- 35 5) Autophagy-deficient mice die from cachexia mediated by appetite loss
- 36 6) Degenerative conditions due to impaired autophagy are caused by the inflammatory response
- 37 to the damage
- 38 7) Targeting CCL2 may be a viable approach to prevent degenerative wasting disorders

39     **Abstract**

40     Macroautophagy (autophagy hereafter) captures intracellular components and delivers them to  
41     lysosomes for degradation and recycling<sup>1</sup>. In adult mice, autophagy sustains metabolism to  
42     prevent wasting by cachexia and to survive fasting, and also suppresses inflammation, liver  
43     steatosis, neurodegeneration, and lethality<sup>2,3</sup>. Defects in autophagy contribute to metabolic,  
44     inflammatory and degenerative diseases, however, the specific mechanisms involved were  
45     unclear<sup>4</sup>. Here we profiled metabolism and inflammation in adult mice with conditional, whole-  
46     body deficiency in an essential autophagy gene and found that autophagy deficiency altered fuel  
47     usage, and reduced ambulatory activity, energy expenditure, and food intake, and elevated  
48     circulating GDF15, CXCL10, and CCL2. While deletion of *Gdf15* or *Cxcl10* provided no or mild  
49     benefit, deletion of *Ccl2* restored food intake, suppressed cachexia and rescued lethality of  
50     autophagy-deficient mice. To test if appetite suppression by CCL2 was responsible for lethal  
51     cachexia we performed single nucleus RNA sequencing of the hypothalamus, the center of  
52     appetite control in the brain. Notably, we found that autophagy deficiency was specifically toxic  
53     to PMCH and HCRT neurons that produce orexigenic neuropeptides that promote food intake,  
54     which was rescued by deficiency in CCL2. Finally, the restoration of food intake via leptin  
55     deficiency prevented lethal cachexia in autophagy-deficient mice. Our findings demonstrate a  
56     novel mechanism where autophagy prevents induction of a cachexia factor, CCL2, which  
57     damages neurons that maintain appetite, the destruction of which may be central to degenerative  
58     wasting conditions.

59  
60     **Main**

61     Autophagy is regulated by the autophagy-related genes (*Atg*) that function to assemble  
62     autophagosomes and capture cargo including intracellular proteins and organelles, for degradation  
63     and recycling. Macromolecules produced by autophagy recycling support metabolism and  
64     eliminate damaged proteins and organelles thereby suppressing inflammation<sup>5,6</sup>. Autophagy  
65     recycling is essential for cell survival in mammals during the absence of nutrients. *Atg5-* or *Atg7-*  
66     deficient mice are born developmentally normal but fail to survive the neonatal starvation period  
67     due, in part, to nutrient insufficiency<sup>1,7</sup>. Moreover, fasting is lethal to adult mice with conditional,  
68     whole-body deletion of *Atg5* or *Atg7* due to hypoglycemia and wasting of muscle and adipose

69 tissue characteristic of cachexia<sup>2,3</sup>. Thus, the evolutionary conserved function of autophagy is  
70 sustaining metabolic homeostasis and survival to nutrient deprivation.

71  
72 Autophagy is also important in the fed state, however, the specific mechanisms are unclear.  
73 Conditional ablation of *Atg5* or *Atg7* in adult mice leads to liver inflammation and  
74 neurodegeneration, and also weight loss, adipose tissue lipolysis and muscle atrophy, and body  
75 wasting characteristic of cachexia<sup>2,3,8</sup>. The lifespan of adult mice with conditional deficiency in  
76 autophagy is limited to less than 3 months<sup>2,3</sup>. Interestingly, neuronal-specific *Atg5* expression  
77 rescues the neonatal lethality of *Atg5*-deficient mice<sup>7</sup>, however, the aspect of neuronal function  
78 that is required to enable survival and if or how this is related to cachexia is unknown<sup>9</sup>. We found  
79 that autophagy suppresses CCL2 thereby preserving hypothalamic neurons and food intake, which  
80 prevents lethal cachexia. Thus, CCL2 is a cachexia factor responsible for hypothalamic neuron  
81 degeneration leading to anorexia and death.

82

### 83 **Results**

#### 84 **Autophagy deficiency leads to weight loss, altered body composition, liver inflammation, 85 and cachexia**

86 To investigate the role of autophagy in whole-body metabolism and cachexia, we analyzed body  
87 composition in conditional whole-body *Atg7*-deficient (*Atg7*<sup>Δ/Δ</sup>) compared to autophagy-intact  
88 (*Atg7*<sup>+/+</sup>) mice. At ten weeks post-deletion, *Atg7*<sup>Δ/Δ</sup> mice showed consistent reduction in body  
89 weight and a greater percent decrease from their initial body weight (Fig. 1a, S1a). *Atg7*<sup>Δ/Δ</sup> mice  
90 also exhibited reduced lean mass, progressive fat mass depletion (Fig. 1b-c) with lower weights  
91 of white and brown adipose tissue, as well as soleus and gastrocnemius plantaris muscles,  
92 compared to *Atg7*<sup>+/+</sup> mice (S1b-c). Previous studies have shown that short-term  
93 conditional *Atg7* deletion results in liver inflammation, steatosis, and hepatomegaly<sup>2,10,11</sup>. At ten  
94 weeks post-deletion, when liver weight was excluded from body weight, a further reduction in  
95 weight was observed in *Atg7*<sup>Δ/Δ</sup> mice (Fig. 1d). Thus, the reduction in body weight seen in  
96 *Atg7*<sup>Δ/Δ</sup> mice is an underestimate of body wasting due to the enlarged liver. In *Atg7*<sup>Δ/Δ</sup> mice,  
97 serum levels of liver enzymes alanine aminotransferase (ALT) and aspartate aminotransferase  
98 (AST) were elevated, indicating liver inflammation and impaired function (Fig. S1d). To explore  
99 the relationship between weight loss, systemic inflammation, and autophagy deficiency, we

100 performed RNA sequencing on livers from *Atg7<sup>Δ/Δ</sup>* mice and compared them to *Atg7<sup>+/+</sup>* controls  
101 (Fig. S1e). GSTA1, GSTM1, and GSTM3 are genes encoding Glutathione S-Transferases  
102 (GSTs), which play a key role in oxidative stress response and detoxification by conjugating  
103 reduced glutathione to toxins, were significantly upregulated in the livers of *Atg7<sup>Δ/Δ</sup>* mice.  
104 Moreover, expression of two pro-inflammatory cytokines, CXCL10 and CCL2 were upregulated  
105 in *Atg7<sup>Δ/Δ</sup>* mice liver consistent with the known role of autophagy in suppressing damage and  
106 inflammation in the liver<sup>2,12</sup>.

107  
108 To monitor metabolic activity in *Atg7<sup>Δ/Δ</sup>* and *Atg7<sup>+/+</sup>* mice they were assessed in metabolic cages  
109 every two weeks post-deletion. Conditional whole-body *Atg7*-deficient mice and mice  
110 lacking *Atg7* specifically in the central nervous system present with abnormal limb-clasping  
111 reflexes and behavioral defects<sup>2,13,14</sup>. Accordingly, we measured behavioral activity through  
112 ambulatory activity and total wheel running and found *Atg7<sup>Δ/Δ</sup>* mice displayed lower activity  
113 compared to *Atg7<sup>+/+</sup>* mice (Fig. e-f). Ambulatory activity analysis revealed a significant decrease  
114 at each timepoint in *Atg7<sup>Δ/Δ</sup>* mice (Fig. S1f). These findings are consistent with neurodegeneration  
115 attributed to deficient autophagy<sup>15</sup>.

116  
117 The respiratory exchange ratio (RER), which represents the ratio of produced CO<sub>2</sub> to consumed  
118 O<sub>2</sub> is reflective of the major types of macronutrients being metabolized (lipids vs. carbohydrates).  
119 Hourly RER plots at 2- and 8-weeks post-deletion revealed that *Atg7<sup>Δ/Δ</sup>* mice exhibited higher RER  
120 values compared to *Atg7<sup>+/+</sup>* mice during the dark phase when mice are active (Fig. 1g). RER  
121 analysis across both light and dark phases showed that this increase was statistically significant  
122 during the dark phase at each time point (Fig. 1h, S1g). These findings suggest a shift away from  
123 fat and/or toward carbohydrate (glucose) utilization as the preferred fuel source. This observation  
124 aligns with previous studies showing glycogen depletion in the liver of adult mice with conditional  
125 autophagy deficiency<sup>2,16</sup> and may indicate a compensatory reliance on alternative nutrient sources  
126 due to a metabolic deficit. In contrast, no differences were observed between *Atg7<sup>Δ/Δ</sup>* and  
127 *Atg7<sup>+/+</sup>* mice during the light phase for RER when mice are inactive (Fig. 1h, S1g).

128  
129 Involuntary weight loss is often linked to reduced appetite and/or increased energy expenditure,  
130 which disrupts energy homeostasis. Total energy expenditure (TEE), which encompasses basal

131 metabolism, thermoregulation, physical activity, and the thermic effect of food intake, was reduced  
132 in *Atg7<sup>Δ/Δ</sup>* mice, failing to account for weight loss (Fig. 1i). Remarkably, we found that  
133 *Atg7<sup>Δ/Δ</sup>* mice exhibited significantly lower food intake compared to *Atg7<sup>+/+</sup>* mice (Fig. 1j),  
134 surprising given that they are intolerant to fasting, but possibly explaining loss of lean and fat  
135 mass. As cytokines and chemokines can regulate appetite<sup>17,18</sup> we measured these factors in the  
136 serum (Fig. S1h). We found three factors that were significantly upregulated in the circulation of  
137 *Atg7<sup>Δ/Δ</sup>* mice compared to *Atg7<sup>+/+</sup>* mice: Growth differentiation factor 15 (GDF15), C-X-C motif  
138 chemokine ligand 10 (CXCL10), and C-C motif ligand 2 (CCL2) (Fig. 1k). Thus, autophagy-  
139 deficient mice display a cachexia-like syndrome, including loss of body weight, appetite, and  
140 wasting of muscle and fat, and increased levels of circulating cytokines and chemokines.

141

#### 142 **CCL2 is the dominant factor responsible for lethal cachexia in autophagy-deficient mice**

143 To determine if GDF15, CXCL10 or CCL2 contribute to cachexia in autophagy-deficient mice,  
144 we generated double knockout mice for each factor on the conditional *Atg7<sup>Δ/Δ</sup>* background. GDF15  
145 is a hormone known to reduce food intake<sup>19,20</sup> by causing food aversion via signaling through  
146 specific neurons in the area postrema and the nucleus of the solitary tract that express its receptor  
147 GFRAL<sup>21,22</sup>. To determine whether GDF15 modulates the lethality in autophagy deficiency, we  
148 generated mice with constitutive deficiency in *Gdf15*<sup>23,24</sup> and crossed them to *Ubc-Cre<sup>ERT2/+</sup>*;  
149 *Atg7<sup>flox/flox</sup>* mice to generate *Gdf15<sup>-/-</sup>*; *Ubc-Cre<sup>ERT2/+</sup>*; *Atg7<sup>flox/flox</sup>* mice. Tamoxifen (TAM)  
150 administration was used to delete *Atg7* in the presence and absence of GDF15 (Fig. S1i). The loss  
151 of GDF15, however, neither rescued the lethality caused by autophagy deficiency (Fig. S1i) nor  
152 did it impact any other obvious phenotype.

153

154 CXCL10 is a chemokine induced in association with metabolic diseases<sup>25</sup> and infection<sup>25-27</sup>. To  
155 investigate whether CXCL10 induction contributed to altered metabolism and reduced survival  
156 caused by autophagy deficiency, mice with constitutive deficiency in *Cxcl10*<sup>27</sup> were crossed  
157 with *Ubc-Cre<sup>ERT2/+</sup>*; *Atg7<sup>flox/flox</sup>* mice to generate *Cxcl10<sup>-/-</sup>*; *Ubc-Cre<sup>ERT2/+</sup>*; *Atg7<sup>flox/flox</sup>* mice. TAM  
158 administration was used to delete *Atg7* in the presence and absence of CXCL10 (Fig. S1j).  
159 *Cxcl10<sup>-/-</sup>; Atg7<sup>Δ/Δ</sup>* mice demonstrated a small but significant improvement in survival compared to  
160 *Atg7<sup>Δ/Δ</sup>* mice, with median survival increased from 64 days to 134 days (Fig. S1j). These results  
161 suggest that CXCL10 modestly extends survival, but neither GDF15 nor CXCL10 deficiency is

162 sufficient to substantially rescue weight loss, food intake, and lethality resulting from autophagy  
163 deficiency.

164  
165 CCL2 is a chemokine that recruits monocytes, macrophages, and other immune cells to sites of  
166 injury or infection<sup>23,28</sup>. It has been previously implicated in cancer-induced cachexia<sup>29</sup>, specifically  
167 metabolic changes in muscle and white adipose tissue (WAT)<sup>30</sup>. To test whether CCL2 impacts the  
168 survival of mice lacking autophagy, mice with constitutive deficiency in *Ccl2*<sup>23</sup> were crossed  
169 with *Ubc-Cre*<sup>ERT2/+</sup>; *Atg7*<sup>flox/flox</sup> mice to generate *Ccl2*<sup>-/-</sup>; *Ubc-Cre*<sup>ERT2/+</sup>; *Atg7*<sup>flox/flox</sup> mice. TAM  
170 administration was used to delete *Atg7* in the presence and absence of CCL2 (Fig. 2Sa). While  
171 *Atg7*<sup>Δ/Δ</sup> mice survived less than three months<sup>2</sup>, the loss of CCL2 completely rescued lethality  
172 induced by autophagy deficiency (Fig. 2a). Notably, loss of CCL2 did not induce major alterations  
173 in the cytokine and chemokine profile comparing *Atg7*<sup>Δ/Δ</sup> and *Atg7*<sup>+/+</sup> mice, suggesting that it may  
174 function directly (Fig. S2b).

175  
176 To determine how eliminating CCL2 rescued lethality of autophagy-deficient mice we  
177 characterized the phenotypes of the four mouse genotypes. Histologic examination of tissues by  
178 H&E showed that CCL2 deficiency mitigated tissue damage resulting from loss of autophagy  
179 including liver inflammation, depletion of the lipid content of white adipose tissue (WAT) and  
180 brown adipose tissue (BAT), and atrophy of skeletal muscle (Fig. S2c). Notably, the physical  
181 appearance of cachexia, the increased livers weights, and the impaired liver function was  
182 diminished in the *Ccl2*<sup>-/-</sup>; *Atg7*<sup>Δ/Δ</sup> compared to *Atg7*<sup>Δ/Δ</sup> mice (Fig. 2b, Sd-e). While *Atg7*<sup>Δ/Δ</sup> mice  
183 develop evidence of severe hepatic dysfunction, as assessed by hyperbilirubinemia, low  
184 triglyceride levels, and low blood urea nitrogen (BUN), the *Ccl2*<sup>-/-</sup>; *Atg7*<sup>Δ/Δ</sup> mice were protected  
185 (Fig. S2f). Together, these results suggested that CCL2 plays a crucial role in maintaining survival  
186 and preventing tissue damage upon loss of autophagy.

187  
188 CCL2 induction is associated with weight loss including depleting muscle and adipose tissue while  
189 also inducing liver steatosis<sup>29</sup>, particularly during systemic inflammation<sup>31</sup> and  
190 neurodegeneration<sup>32</sup> similar to what we observed in autophagy-deficient animals. As such,  
191 therapeutic targeting of CCL2 with antibodies was attempted, but unfortunately without success<sup>33</sup>.  
192 To test if inhibiting CCL2 with an antibody was equivalent to genetic *Ccl2* deficiency we

193 regenerated the C1142 monoclonal antibody (mAb) proposed to neutralize circulating CCL2<sup>34,35</sup>.  
194 Following TAM-induced autophagy deficiency, mice were treated with either C1142 mAb or an  
195 IgG control antibody. While *Atg7<sup>Δ/Δ</sup>* mice treated with either C1142 mAb or IgG mAb showed no  
196 difference in survival (Fig. S2g), the *Atg7<sup>Δ/Δ</sup>* mice treated with C1142 mAb showed partial rescue  
197 of body weight over time compared to IgG mAb (Fig. S2h). However, this result was due to an  
198 increase in lean mass from further increased hepatomegaly in *Atg7<sup>Δ/Δ</sup>* mice rather than a prevention  
199 of adipose and skeletal muscle wasting (Fig. S2i). These data suggest that an antibody directed  
200 against a CCL2 peptide does not phenocopy genetic deletion of *Ccl2*. Notably, CCL2 levels in the  
201 liver of *Atg7<sup>Δ/Δ</sup>* mice treated with C1142 mAb showed a decreasing trend compared to IgG-treated  
202 mice, although no significant (Fig. S2j). These observations are in agreement with previous clinical  
203 trial observations with therapeutic anti-CCL2 candidates that similarly failed to deplete the  
204 chemokine<sup>36</sup>. Moreover, they suggest that previous attempts to target CCL2 with an antibody *in vivo*  
205 were likely ineffective and perhaps counterproductive.

206

### 207 **Loss of CCL2 rescues fasting lethality by preserving liver gluconeogenesis**

208 The loss of CCL2 extends lifespan and attenuates tissue damage in *Atg7<sup>Δ/Δ</sup>* mice (Fig. 2a,S2c).  
209 Therefore, we sought to investigate if elevated CCL2 levels also contributed to the fasting-induced  
210 mortality due to hypoglycemia in autophagy-deficient mice<sup>2,3</sup> Mice were subjected to fasting (free  
211 access to water without food for 24 hours). In contrast to the *Atg7<sup>Δ/Δ</sup>* mice that die upon fasting,  
212 *Ccl2<sup>-/-</sup>;Atg7<sup>Δ/Δ</sup>* mice survive (Fig. 2c). Blood glucose and serum insulin levels during fasting were  
213 maintained in *Ccl2<sup>-/-</sup>;Atg7<sup>Δ/Δ</sup>* compared to *Atg7<sup>Δ/Δ</sup>* mice, which present with hypoglycemia and  
214 reduced insulin levels (Fig. 2d). We hypothesized that elevated blood glucose levels in  
215 *Ccl2<sup>-/-</sup>;Atg7<sup>Δ/Δ</sup>* compared to *Atg7<sup>Δ/Δ</sup>* mice resulted from preservation of liver function and the  
216 ability to perform gluconeogenesis during fasting. To test this hypothesis, we measured  
217 gluconeogenesis by injecting mice with L-Lactate and then measuring the resulting glucose levels  
218 in the blood. *Atg7<sup>Δ/Δ</sup>* mice showed impaired ability to utilize lactate for glucose synthesis compared  
219 to *Ccl2<sup>-/-</sup>;Atg7<sup>Δ/Δ</sup>* mice, which maintained this capacity (Fig. 2e). To confirm that loss of CCL2  
220 restored hepatic gluconeogenesis in autophagy-deficient mice, we performed *in vivo* <sup>13</sup>C lactate  
221 tracing. The labeled lactate in the plasma of *Atg7<sup>Δ/Δ</sup>* mice was significantly higher as compared to  
222 *Ccl2<sup>-/-</sup>;Atg7<sup>Δ/Δ</sup>* mice (Fig. 2f), while the plasma glucose enrichment levels remained unchanged  
223 between the groups (Fig. 2h). However, the ratio of glucose to lactate showed that significantly

224 less lactate was being converted to glucose in *Atg7<sup>Δ/Δ</sup>* compared to *Ccl2<sup>-/-</sup>;Atg7<sup>Δ/Δ</sup>* mice (Fig. 2i).  
225 These findings demonstrated that *Atg7<sup>Δ/Δ</sup>* mice are unable to efficiently utilize circulating lactate  
226 for gluconeogenesis, resulting in reduced blood glucose levels and lethality upon fasting due to  
227 hepatic dysfunction. In contrast, *Ccl2<sup>-/-</sup>;Atg7<sup>Δ/Δ</sup>* mice effectively convert lactate to glucose via  
228 gluconeogenesis, maintaining blood glucose levels and animal survival during fasting.

229

230 **CCL2 deficiency rescues weight and food intake but not fuel utilization or ambulatory  
231 activity**

232 In contrast to *Atg7<sup>Δ/Δ</sup>* mice, *Ccl2<sup>-/-</sup>;Atg7<sup>Δ/Δ</sup>* mice maintained body weight, lean mass, and fat mass  
233 (Fig. 3a-c) in addition to survival. Interestingly, *Ccl2<sup>-/-</sup>* mice presented with a larger initial body  
234 weight, gained significantly more weight compared to the other genotypes, and accumulate larger  
235 lipid deposits in adipose tissues compared to *Atg7<sup>+/+</sup>* mice (Fig. 3a-c, S2c). Together these results  
236 suggest a role for CCL2 in regulating body composition.

237

238 Metabolic phenotyping found *Ccl2<sup>-/-</sup>;Atg7<sup>Δ/Δ</sup>* and *Atg7<sup>Δ/Δ</sup>* mice showed no significant difference  
239 in the RER, suggesting nutrient utilization and preference was similar (Fig. 3e-f). Ambulatory  
240 activity also showed no significant difference between *Ccl2<sup>-/-</sup>;Atg7<sup>Δ/Δ</sup>* compared to *Atg7<sup>Δ/Δ</sup>* mice  
241 (Fig. 3d) and there was partial rescue in progressive motor, ataxia, and behavioral deficits in  
242 *Ccl2<sup>-/-</sup>;Atg7<sup>Δ/Δ</sup>* compared to *Atg7<sup>Δ/Δ</sup>* mice (Fig. S2k) and Supplementary Movie S1. Brain  
243 histological analyses showed the numbers of pyramidal neurons and Purkinje cells, related to  
244 motor function and coordinated movement, were significantly increased in  
245 *Ccl2<sup>-/-</sup>;Atg7<sup>Δ/Δ</sup>* compared to *Atg7<sup>Δ/Δ</sup>* mice (Fig. S2l). These results indicated that induction of  
246 CCL2 in autophagy deficient mice was not responsible for altered RER or defective ambulatory  
247 activity although there was some preservation of Purkinje cells in the cerebellum and some  
248 mitigation of defective hindlimb clasping. Eliminating CCL2, therefore, does not rescue all  
249 autophagy-defect related phenotypes and would not be expected to correct cell damage induced  
250 by failure of protein and organelle clearance critical to the function of post-mitotic and motor  
251 neurons<sup>37</sup>.

252

253 As shown above, *Atg7<sup>Δ/Δ</sup>* mice have decreased food intake, TEE, and high levels of CCL2. We  
254 therefore measured TEE and food intake in *Ccl2<sup>-/-</sup>* and *CCL2<sup>-/-</sup>; Atg7<sup>Δ/Δ</sup>* mice. Loss of CCL2

255 restored TEE comparable to *Atg7<sup>+/+</sup>* mice (Fig. 3g). Interestingly, *Ccl2<sup>-/-</sup>* mice exhibited increased  
256 food consumption during the dark and light cycle when compared to *Atg7<sup>+/+</sup>* mice (Fig. 3h).  
257 Surprisingly, loss of CCL2 significantly preserved food intake in *Ccl2<sup>-/-</sup>;Atg7<sup>Δ/Δ</sup>* mice compared to  
258 *Atg7<sup>Δ/Δ</sup>* mice at both 2- and 8-weeks post deletion. (Fig. 3h). These results suggest that CCL2  
259 induction in autophagy-deficient mice inhibited appetite, decreased food intake, and disrupted  
260 energy homeostasis, which would be potentially lethal as they are intolerant to fasting.

261

## 262 **Eliminating CCL2 rescues loss of appetite-promoting hypothalamic neurons**

263 The ability of CCL2 deficiency to preserve food intake in autophagy-deficient mice suggested that  
264 CCL2 may be toxic to neurons in the hypothalamus that express its cognate receptor, CCR2, and  
265 produce hormones that regulate food intake<sup>38</sup>. To test this hypothesis, single nucleus RNA  
266 sequencing (snRNA-seq) was applied to the hypothalamus from wild-type and *Ccl2<sup>-/-</sup>* mice with  
267 and without deletion of *Atg7*. The hypothalami were pooled with four samples per genotype due  
268 to the low weight of the tissue. This analysis yielded 20,297 high-quality single-nucleus  
269 transcriptomes (Fig. 4a, S3a). Using molecular markers of known hypothalamic regions and cell  
270 types<sup>39</sup>, we were able to annotate the major hypothalamic cell type populations for each of the four  
271 mouse genotypes (Fig. 4b). We identified 52 clusters that were classified into 28 broad cell types,  
272 including astrocytes, fibroblast, oligodendrocytes, GABAergic (GABA) and glutamatergic (GLU)  
273 neurons (Fig. 4b). UMAP embedding of each model is also shown (Fig. 4c, S3b). UMAP  
274 embedding of each model is also shown (Fig. 4c, S3b). Notably, a cell subpopulation forming  
275 Cluster 4 did not match to any known cell types from prior studies (Fig. 4a)<sup>39</sup>. Cells in Cluster 4  
276 had a higher level of mitochondrial gene expression and lower overall snRNA-seq signal than  
277 other clusters, suggesting they were more likely apoptotic (Fig. S3c). Cluster 4 cells were  
278 predominately from the *Atg7<sup>Δ/Δ</sup>* hypothalamus (Fig. 4c,d), as compared with the remaining clusters  
279 which had a relatively even distribution across the four genotypes. Note that CCL2 expression was  
280 predominantly in the fibroblast cluster in *Atg7<sup>Δ/Δ</sup>* mice (Fig. 4e). These findings suggest that  
281 Cluster 4 may represent cells in the hypothalamus that are negatively impacted by loss of  
282 autophagy and that are restored by co-deletion of *Ccl2*.

283

284 Positive logFC values in Cluster 4 had significant upregulation of hypocretin (Hcrt), which  
285 encodes the neuropeptide orexin, and pro-melanin-concentrating hormone (Pmch), the precursor

286 gene that encodes the neuropeptide melanin-concentrating hormone (MCH) (Fig.4f). Both orexin  
287 and pro-MCH are orexigenic hormones that stimulate appetite. To validate the snRNA-seq gene  
288 expression analysis from Cluster 4, qRT-PCR analysis was used to measure pro-MCH mRNA  
289 expression in the hypothalamus. Hypothalami from *Atg7<sup>Δ/Δ</sup>* mice had decreased mRNA expression,  
290 while *Ccl2<sup>-/-</sup>;Atg7<sup>Δ/Δ</sup>* mice had restored mRNA expression similar to *Atg7<sup>+/+</sup>* and *Ccl2<sup>-/-</sup>* mice  
291 (Fig. S3d). This data suggested that loss of autophagy leads to CCL2-dependent degradation of  
292 cells represented by Cluster 4, which is composed of neurons that produce pro-MCH and orexins,  
293 both orexigenic neuropeptides. Thus, the CCL2-induced defective food intake in *Atg7<sup>Δ/Δ</sup>* mice may  
294 be due to degradation of neurons that produce positive regulators of appetite, the loss of which  
295 may be lethal (Fig. 4g).

296

### 297 **Preservation of appetite rescues survival of autophagy-deficient mice**

298 To test the hypothesis that inhibition of food intake was lethal to autophagy-deficient mice we  
299 evaluated if eliminating leptin, an appetite suppressing hormone that signals through the  
300 hypothalamus, could rescue their defective food intake and survival. Leptin-deficient humans and  
301 mice are obese due to their inability to suppress appetite and food intake<sup>40</sup>. Leptin deficient (*ob/ob*)  
302 mice<sup>41</sup> were crossed with *Ubc-Cre<sup>ERT2/+</sup>;Atg7<sup>fl/fl</sup>* mice to generate *ob/ob;Ubc-*  
303 *Cre<sup>ERT2/+</sup>;Atg7<sup>fl/fl</sup>* mice. TAM administration was used to delete *Atg7* in the presence or absence  
304 of leptin. Leptin deficiency rescued lethality of autophagy deficient *ob/ob;Atg7<sup>Δ/Δ</sup>* mice, which  
305 survived >250 days post deletion (Fig. 5a). Representative images of each mouse genotype show  
306 the weight distribution between respective groups (Fig. 5b). *ob/ob* and *ob/ob;Atg7<sup>Δ/Δ</sup>* mice had  
307 similar obese body weights, and fat mass compared to cachectic *Atg7<sup>Δ/Δ</sup>* mice (Fig. 5c,d). Lean  
308 mass was comparable between *ob/ob;Atg7<sup>Δ/Δ</sup>* and *Atg7<sup>Δ/Δ</sup>* mice. (Fig. 5e). Additionally, the levels  
309 CCL2 were comparable in *ob/ob;Atg7<sup>Δ/Δ</sup>* and *Atg7<sup>Δ/Δ</sup>* mice indicating that leptin deficiency does  
310 not rescue survival of autophagy-deficient mice by eliminating CCL2 (Fig. 5f). Leptin deficiency  
311 also rescued fasting lethality of autophagy-deficient mice due to the rescue of hypoglycemia and  
312 cachexia (Fig. 5g). Lastly, food intake was also rescued in *ob/ob;Atg7<sup>Δ/Δ</sup>* and *Atg7<sup>Δ/Δ</sup>* mice (Fig.  
313 5h). Thus, autophagy-deficient mice die due to CCL2-mediated suppression of appetite and food  
314 intake that can be rescued by increasing appetite and food intake by deleting leptin (Fig. 5i). As  
315 autophagy-deficient mice fail to survive fasting, loss of appetite and food intake is lethal.

316

317 **Discussion**

318 CCL2 is induced in activated microglia in neuroinflammatory diseases and its transgenic  
319 expression in mice is sufficient to produce neuronal damage. CCL2 and its receptor CCR2 are  
320 associated with STAT2 and IL1 $\beta$  activation and neurodegeneration<sup>32,42,43</sup>, but the mechanisms  
321 involved are unclear. CCL2 is also associated with cachexia in cancer models. Administration of  
322 CCL2 to mice induces wasting of skeletal muscle<sup>44</sup> and recruitment of macrophages by CCL2 to  
323 tumors promotes cachexia<sup>45</sup>, by unknown mechanisms. The lack of food intake in the *Atg7*-  
324 deficient mice is associated with anorexia mediated in the hypothalamus. This is distinct from the  
325 effect that GDF15 and the inflammatory cytokine IL-6 that seem to mediate anorexia via receptors  
326 in the area postrema.

327

328 The chronic loss of the rat MCH-precursor *Pmch* decreases food intake<sup>46,47</sup> and also affects energy  
329 expenditure<sup>46</sup>, thus providing insight into the changed body weight dynamics during chronic loss  
330 of *Pmch*. These findings are consistent with loss of autophagy promoting damage,  
331 neuroinflammation and CCL2 that destroys MCH-producing orexigenic neurons in the  
332 hypothalamus that drive cachexia. Our findings also suggest that targeting CCL2 for degenerative  
333 diseases needs to be reexamined due to technical limitations of the approaches in the past.  
334 Cachexia is a feature of neurodegenerative and other unresolvable diseases<sup>48,49</sup>. Our findings  
335 provide powerful evidence that CCL2 is a cachectic factor that works by suppressing appetite by  
336 inhibiting neurons that produce orexigenic peptides. Clear demonstration that CCL2-induced loss  
337 of appetite causes lethal cachexia derived from our ability to restore appetite, prevent weight loss  
338 and rescue lethal cachexia by eliminating leptin.

339

340 Autophagy protects from numerous degradative and inflammatory diseases, and this knowledge  
341 has provoked efforts to enhance autophagy for therapeutic benefit<sup>50</sup>. Our findings reveal that much  
342 of the damage from autophagy inhibition is surprisingly mediated by CCL2. The orexigenic MCH  
343 neurons that are the target of CCL2 express a CCL2 receptor, CCR2<sup>38</sup>, but not CCL2 itself. Thus,  
344 loss of autophagy that triggers production of CCL2 occurs in cells other than the HCRT and MCH  
345 neurons themselves, perhaps in fibroblasts within the hypothalamus or in activated microglia.  
346 These findings also suggest that tissue damage, for example through inhibition of autophagy as  
347 shown here, is greatly amplified by the ensuing inflammatory response to that damage. Thus,

348 limiting or resolving the inflammatory response rather than trying to prevent the damage is an  
349 alternative approach to mitigate neurodegeneration and other degenerative conditions. Finally, we  
350 demonstrate how destructively lethal cachexia can be, as autophagy-deficient mice, despite having  
351 several other afflictions, die because they stop eating, illustrating the importance of addressing  
352 mechanisms underlying cachexia.

353

354

355

356

357

358

359

360

361

362

363

364

365 **Author contributions**  
366 MI designed, performed genomic data analysis. MGJ, A. Sawant, ECL, and ETM assisted with  
367 mice experiments. JA-S and SMD produced and generated C1142 antibody. ZH assisted with  
368 maintaining mouse colonies, ear tagging and antibody treatments. AD, MS, and SS assisted with  
369 genotyping. JDR, XS, TGA, MDG, and TJ provided data analysis, result interpretation, and  
370 contributed valuable suggestions. YP, A. Scheinfeld, and ZZ supported the sequencing,  
371 interpreted results, and assisted with writing. EW conceived and supervised the study. All authors  
372 read, edited, and approved the manuscript.  
373

374 **Acknowledgements**  
375 This work was supported by the Ludwig Institute for Cancer Research, Ludwig Princeton  
376 Branch, Princeton University of EW, and Cancer Grand Challenges CGCSDF-2021\100003  
377 (CRUK) and 1OT2CA278609-01 (NCI) to EW, MDG and TJ, and NIH grant R01 CA163591 to  
378 EW, JDR, and NIH grant R01 CA243547 to EW, and NIH grant DP2 AI171161 awarded to Y.P.  
379 MI was also supported by postdoctoral fellowship COCR23PRF005 from New Jersey  
380 Commission on Cancer Research (NJCCR), MG-J was also supported by 1T32CA257957, ECL  
381 was supported by R01 CA243547, and A. Sawant was supported by postdoctoral fellowship  
382 DFHS10PPC029 from NJCCR. We thank Rutu Patel, Suman Amjad, Angelina Gruszecki, and  
383 Ann Hinrichs for their help with genotyping. SMD and JA-S (LAbCore) were funded directly by  
384 Ludwig Cancer Research. We acknowledge support from the Rutgers Cancer Institute  
385 Metabolomics Shared Resource (NCI-CCSG P30CA072720-6852), the Biospecimen Repository  
386 and Histopathology Service Shared Resource (P30CA072720-5919), and the Immune  
387 Monitoring and Flow Cytometry Shared Resource, supported, in part, with funding from NCI-  
388 CCSG P30CA072720-6852. The schematic representations were created using BioRender.com.  
389 The authors also acknowledge the support from all members of the White laboratory.  
390

391 **Materials and Methods**  
392 **Mouse Models**  
393 All animal care was carried out in compliance with Rutgers University Institutional Animal Care  
394 and Use Committee guidelines (IACUC). Ubc-Cre<sup>ERT2/+</sup> mice<sup>51</sup> (The Jackson Laboratory) and  
395 Atg7<sup>flox/flox</sup> mice<sup>1</sup> (provided by Dr. M. Komatsu, Tokyo Metropolitan Institute of Medical

396 Science) were cross-bred to generate the Ubc-Cre<sup>ERT2/+</sup>; Atg7<sup>flox/flox</sup> mice as previously described  
397 <sup>2</sup>To generate Ubc-Cre<sup>ERT2/+</sup>; Atg7<sup>flox/flox</sup>; Ccl2<sup>-/-</sup>, Ccl2<sup>-/-</sup><sup>23</sup> (The Jackson Laboratory) were cross-  
398 bred with our previously created Ubc-Cre<sup>ERT2/+</sup>; Atg7<sup>flox/flox</sup> mice. To generate Ubc-Cre<sup>ERT2/+</sup>;  
399 Atg7<sup>flox/flox</sup>; Cxcl10<sup>-/-</sup>, CXCL10<sup>-/-</sup><sup>27</sup> (The Jackson Laboratory) were cross-bred with our  
400 previously created Ubc-Cre<sup>ERT2/+</sup>; Atg7<sup>flox/flox</sup> mice. To Ubc-Cre<sup>ERT2/+</sup>; Atg7<sup>flox/flox</sup>; Lep<sup>ob</sup>/Lep<sup>ob</sup>,  
401 Lep<sup>ob</sup>/Lep<sup>ob</sup><sup>52</sup> (The Jackson Laboratory) were cross-bred with our previously created Ubc-Cre  
402 ERT2<sup>+/+</sup>; Atg7<sup>flox/flox</sup> mice.

#### 403 **Tamoxifen Preparation and Administration**

404 TAM (T5648, Sigma) was suspended at a concentration of 20 mg/ml, in a mixture of 98%  
405 sunflower seed oil and 2% ethanol. For TAM delivery, 200 µl per 20 g of body weight (20mg/kg)  
406 were injected intraperitoneally into 8 to 10 weeks old mice. Mice were treated once per day for 4  
407 days to delete floxed gene systematically<sup>2</sup>. Ubc-Cre<sup>ERT2/+</sup>; Atg7<sup>flox/flox</sup>; Lep<sup>ob</sup>/Lep<sup>ob</sup> were treated  
408 twice per week for 2 weeks.

#### 409 **Survival**

410 For mouse Kaplan-Meyer survival curve, mice were monitored daily until they reached the  
411 endpoint. The criteria for euthanization were a body condition score of 2, body weight loss of  
412 >15%, or natural death.

#### 413 **Fasting**

414 Fasting was conducted as previous described<sup>2</sup>.

#### 415 **Metabolic cages**

416 Two indirect calorimetry systems were used, a 12 cage CLAMS apparatus (Columbus  
417 Instruments) and 16 cage Promethion Core Mouse Metabolic System (Sable System  
418 International). Mice were maintained on a standard chow diet and single housed for 48–72 h  
419 prior to experiment start.  
420 During the experiment, mice were single housed under a 12-hour light-dark cycle at 21C and 55  
421 % humidity for 7 days. The first 24 hours of data collection was removed from analysis due to  
422 acclimation period. Oxygen consumption, CO<sub>2</sub> emission, food consumption, movement, running

423 wheel, and energy expenditure were measured every 15 minutes in the CLAMS and 3 minutes in  
424 the Promethion.

425 Locomotor activity, both horizontal and vertical, was determined by a X, Y, and Z infrared light  
426 beam system. Stationary locomotor activity was defined as continues infrared light beam breaks  
427 of one single light beam and ambulatory movement as continues breaks of two or more different  
428 light beams.

429 Raw data files were collected and processed by the Promethion software package  
430 MacroInterpreter 3, which produced standardized output formats for the metabolic variables of  
431 interest at each cage. The processed data generated by MacroInterpreter 3 was then analyzed by  
432 the CalR: A Web-based Analysis Tool for Indirect Calorimetry Experiments (<https://calrapp.org>)  
433 as described previously<sup>53</sup>.

#### 434 **Body Composition**

435 Body composition analysis (fat and lean mass) was assessed by the EchoMRI™-100H.  
436 Unanesthetized mice were placed in a restraint tube that was inserted into the analyzer for  
437 approximately 2 min. The mouse was then returned to its home cage.

#### 438 **GDF15 ELISA**

439 GDF15 concentration in the serum was determined using a Mouse & Rat GDF-15 ELISA Kit  
440 Quantikine ELISA Kit (R&D Systems; MGD150) according to the manufacturer's instructions.

#### 441 **Cytokine and chemokine assay**

442 Levels of the secreted cytokines and chemokines were determined using the Procarta Plex® 36-  
443 plex immunoassay (Thermo Fischer Scientific; Cat No: EPX360-26092-901) for mouse serum  
444 and liver tissue. Data were collected using a Luminex-200 system and validated using the  
445 xPONENT software package. Aliquots of serum and tissue in duplicate were assayed for the  
446 secreted molecules as per manufacturer's instructions using Luminex 200 System and analyzed  
447 by ProcartaPlex Analyst 1.0 (Luminex Corporation).

448

#### 449 **CCL2 ELISA**

450 CCL2 concentration in the liver tissue supernatants was determined using a Mouse

451 CCL2/JE/MCP-1 Quantikine ELISA Kit (R&D Systems; MJE00B) according to the  
452 manufacturer's instructions.

453 **Production of anti-mCCL2 (C1142)**

454 The complete C1142 mAb (CNTO 888 mouse surrogate) sequence was a kind gift from Janssen  
455 Research and Development, LLC. Briefly, the DNA sequences encoding the IgG2a/kappa heavy  
456 and light chains of C1142, as well as an irrelevant isotype control mAb were synthesized  
457 by a commercial vendor (GeneArt, Invitrogen), with codon optimization for efficient expression  
458 in CHO cells. The ORFs were then sub-cloned separately into customized pTT-based heavy and  
459 light chain episomal expression vectors under the control of cytomegalovirus (CMV) promoters.  
460 Heavy and light chain vectors were co-transfected into ExpiCHO-S cells (Cat. A29133; Gibco)  
461 according to the manufacturer's instructions and expression allowed to proceed for 5 days.  
462 Secreted monoclonal antibodies were purified from clarified expression media using protein A  
463 affinity chromatography with MabSelect beads (Cat. GE17-5199-01; Merck), followed by  
464 extensive dialysis against phosphate-buffered saline (PBS) using Slide-A-Lyzer G2 dialysis  
465 cassettes (Cat. 87731; Life Technologies).

466 **Serum biochemistry analysis**

467 Blood serum samples were analyzed by the Element DC5X™ Veterinary Chemistry Analyzer  
468 (Hesk) performed at Rutgers In Vivo Research Services (IVRS) core facility.

469 **Bulk RNA-seq analysis**

470 At 8 weeks post deletion, liver tissue from *Atg7<sup>+/+</sup>*, *Atg7<sup>Δ/Δ</sup>*, *Ccl2<sup>-/-</sup>*, and *Ccl2<sup>-/-</sup>;Atg7<sup>Δ/Δ</sup>* were  
471 dissected and flash frozen in liquid nitrogen. FastQC v0.11.9  
472 (<https://www.bioinformatics.babraham.ac.uk/projects/fastqc/>) was used to assess sequencing  
473 quality. Reads were first mapped to the mouse genome using HiSat2 v2.2.1<sup>54</sup>. The genomic  
474 index along with the list of splice sites and exons were created by HiSat2 using the genome  
475 assembly mm10 from ENSEMBL together with the comprehensive gene annotation from mm10  
476 vM23 from Gencode<sup>55</sup>. Gene level counts were computed using Rsubread v2.8.2<sup>56</sup> (options  
477 isPairedEnd = TRUE, requireBothEndsMapped = TRUE, minOverlap = 80,  
478 countChimericFragments = FALSE).

479 The liver tissue was analyzed separately, and genes were filtered out from further analysis if the  
480 mean read count across all samples in the tissue was less than 50. This resulted in 10,563,  
481 10,285, and 21,823 genes that went into further analysis of the brown adipose tissue, GNP, and  
482 liver data, respectively. DESeq2 v1.34.0<sup>57</sup> was used to perform differential gene expression  
483 analysis. Differentially expressed genes were used for further analysis and visualization. Gene  
484 expression heatmaps were generated with pheatmap v1.0.12 (<https://cran.r-project.org/web/packages/pheatmap/index.html>) using values that were z-score normalized for  
485 each gene across all samples within each tissue. Volcano plots were generated with  
486 EnhancedVolcano v1.12.0 (<https://github.com/kevinblighe/EnhancedVolcano>). All analysis  
487 starting from count table generation was conducted in the R statistical environment v4.1.3.  
488

489 **snRNA-seq analysis:**

490 At 8 weeks post deletion, hypothalamus tissue from *Atg7<sup>+/+</sup>*, *Atg7<sup>Δ/Δ</sup>*, *Ccl2<sup>-/-</sup>*, and  
491 *Ccl2<sup>-/-</sup>;Atg7<sup>Δ/Δ</sup>* were dissected and flash frozen in liquid nitrogen. Downstream analysis was  
492 carried out using the scanpy package v1.9.3<sup>58</sup>. Initial quality control steps and normalization  
493 were carried out separately for each of the four samples. Cells were filtered out if they had high  
494 relative mitochondrial UMI counts (>4-10% for *Atg7<sup>+/+</sup>*, *Atg7<sup>Δ/Δ</sup>*, *Ccl2<sup>-/-</sup>*, and *Ccl2<sup>-/-</sup>;Atg7<sup>Δ/Δ</sup>*)  
495 and high total counts (>15,000-20,000 for *Atg7<sup>+/+</sup>*, *Atg7<sup>Δ/Δ</sup>*, *Ccl2<sup>-/-</sup>*, and *Ccl2<sup>-/-</sup>;Atg7<sup>Δ/Δ</sup>*), which  
496 resulted in the removal of 150-300 cells for *Atg7<sup>+/+</sup>*, *Atg7<sup>Δ/Δ</sup>*, *Ccl2<sup>-/-</sup>*, and *Ccl2<sup>-/-</sup>;Atg7<sup>Δ/Δ</sup>*. Cells  
497 with the potential of being doublets (score >0.2 as detected by Scrublet, 200-250 cells in each  
498 sample, respectively) were also removed. Genes were filtered out from the subsequent analysis if  
499 they were present in <1% of cells in the sample. Gene expression counts were then normalized  
500 with analytical Pearson residual normalization from scanpy, using a theta value of 10 for all four  
501 of the samples. After normalization, the four samples were concatenated. Non-protein-coding  
502 genes (2,447 genes, 1.6% of total UMI counts) were also filtered out on the basis of the  
503 CellRanger mm10 GTF file vM23. This resulted in a dataset of 20,297 cells and 1,600 genes.

504 PCA was run with 100 components, a kNN graph was built using 30 neighbors, 70 PCs and  
505 cosine metric, and Leiden clustering was carried out with a resolution of 2.1, resulting in 52  
506 clusters. Known marker genes from HypoMap<sup>58</sup> were used to annotate the Leiden clusters using  
507 the score genes function in scanpy and by exploring differentially expressed genes in each cluster  
508 as compared with all cells outside the cluster, obtained using a custom script. For differential

509 expression analysis, log<sub>2</sub> fold change (log<sub>2</sub>FC) of expression was calculated as the ratio of  
510 pseudobulk raw UMI counts summed over cells within and outside the cluster (then normalized  
511 by total amount of UMI counts inside and outside the cluster), p-values were calculated using  
512 Mann-Whitney U test applied to Pearson residual normalized expression values in single cells  
513 within and outside the cluster, and Bonferroni correction for multiple hypothesis testing applied  
514 to all genes with abs(log<sub>2</sub>FC) > 0.5.

## 515 **Tolerance Test**

516 LL-lactate tolerance tests were performed after 6 h of fasting. Mice were injected  
517 intraperitoneally with L-lactate (2 g/kg BW). Blood glucose levels (Accu-Chek Performa  
518 glucometer) were determined from the tail vein at 0, 15, 30, 45, 60, and 120 min after injection  
519 (Accu-Chek Performa glucometer).

## 520 **Histologic and immunohistochemical analysis**

521 Mouse tissues were collected and fixed in 10% formalin solution (Formaldehyde Fresh, Fisher  
522 Scientific, SF94-4). Tissues were fixed overnight and then transferred to 70% ethanol for  
523 paraffin-embedded sections. The slides were deparaffinized, rehydrated and hematoxylin–eosin  
524 staining was performed.

## 525 **Metabolite analysis by LC–MS**

526 Metabolites were extracted as described previously<sup>59</sup>. Briefly, metabolites were extracted from  
527 serum using the extraction buffer containing methanol: acetonitrile: H<sub>2</sub>O (40:40:20). The final  
528 extract was stored at -80 °C until analysis by LC–MS. The LC-MS metabolomic analysis was  
529 performed at the Metabolomics Shared Resource of Rutgers Cancer Institute on a Q Exactive  
530 PLUS hybrid quadrupole-orbitrap mass spectrometer coupled to a Vanquish Horizon UHPLC  
531 system (Thermo Fisher Scientific, Waltham, MA) with an XBridge BEH Amide column (150  
532 mm × 2.1 mm, 2.5 µm particle size, Waters, Milford, MA). The HILIC separation used a  
533 gradient of solvent A (95%:5% H<sub>2</sub>O:acetonitrile with 20 mM acetic acid, 40 mM ammonium  
534 hydroxide, pH 9.4) and solvent B (20%:80% H<sub>2</sub>O:acetonitrile with 20 mM acetic acid, 40 mM  
535 ammonium hydroxide, pH 9.4). The gradient was 0 min, 100% B; 3 min, 100% B; 3.2 min, 90%  
536 B; 6.2 min, 90% B; 6.5 min, 80% B; 10.5 min, 80% B; 10.7 min, 70% B; 13.5 min, 70% B; 13.7  
537 min, 45% B; 16 min, 45% B; 16.5 min, 100% B; and 22 min, 100% B<sup>60</sup>. The flow rate was 300

538  $\mu\text{L}/\text{min}$ . The column temperature was set to 25 °C. The autosampler temperature was set to 4 °C,  
539 and the injection volume was 5  $\mu\text{L}$ . MS scans were obtained in negative ionization mode with a  
540 resolution of 70,000 at m/z 200, in addition to an automatic gain control target of  $3 \times 10^6$  and m/z  
541 scan range of 72 to 1000. Metabolite data was obtained using the MAVEN software package<sup>61</sup>  
542 (mass accuracy window: 5 ppm).

543 **Labelled Lactate infusion**

544 For intra-jugular vein catheterization, the procedure was performed as described previously<sup>59</sup>.  
545 Briefly, venous catheters were surgically implanted into the jugular veins of *Atg7<sup>Δ/Δ</sup>*, *Atg7<sup>+/+</sup>*,  
546 *Ccl2<sup>-/-</sup>*, *Ccl2<sup>-/-</sup>*; *Atg7<sup>Δ/Δ</sup>* mice at 5 weeks post TAM injection. On the day of infusion, mice were  
547 fasted for 6 hours. Mice were infused with 13C-Lactate (CLM-1579-PK) dissolved in sterile  
548 saline at a rate of 0.1  $\mu\text{L}/\text{g}/\text{min}$  for 2.5 hours. Mice were sacrificed after infusion for serum  
549 analysis by LC-MS.

550 **Real-time PCR**

551 Total RNA was isolated from hypothalami by Qiagen RNA micro kit (Qiagen). cDNA was then  
552 reverse transcribed from the total RNA by MultiScribe RT kit (Thermo Scientific). Real-time  
553 PCR were performed on Applied Biosystems StepOne Plus machine using SYBR green master  
554 mix (Thermo Scientific). Results were calculated using  $\Delta\Delta\text{Ct}$  method and then normalized to  
555 actin.

556 **Statistical analysis**

557 Statistical analysis was performed with GraphPad Prism (V.6). A Student's t-test or a one-way  
558 analysis of variance (ANOVA) was used for comparison between the groups. A two-way  
559 ANOVA was used for repeated measures for comparisons between the groups. A post-hoc  
560 comparison using Tukey HSD was applied according to the two-way ANOVA results. Statistical  
561 significance was set at  $p < 0.05$ .

562

563

564

565

566

## References

- 567 1 Komatsu, M. *et al.* Impairment of starvation-induced and constitutive autophagy in Atg7-  
568 deficient mice. *J Cell Biol* **169**, 425-434 (2005). <https://doi.org/10.1083/jcb.200412022>
- 569 2 Karsli-Uzunbas, G. *et al.* Autophagy is required for glucose homeostasis and lung tumor  
570 maintenance. *Cancer Discov* **4**, 914-927 (2014). <https://doi.org/10.1158/2159-8290.CD-14-0363>
- 571 3 Yang, Y. *et al.* Autophagy promotes mammalian survival by suppressing oxidative stress  
573 and p53. *Genes Dev* **34**, 688-700 (2020). <https://doi.org/10.1101/gad.335570.119>
- 574 4 Rabinowitz, J. D. & White, E. Autophagy and metabolism. *Science* **330**, 1344-1348  
575 (2010). <https://doi.org/10.1126/science.1193497>
- 576 5 Mizushima, N. & Komatsu, M. Autophagy: renovation of cells and tissues. *Cell* **147**, 728-  
577 741 (2011). <https://doi.org/10.1016/j.cell.2011.10.026>
- 578 6 Mizushima, N. & Kuma, A. Autophagosomes in GFP-LC3 Transgenic Mice. *Methods Mol Biol* **445**, 119-124 (2008). [https://doi.org/10.1007/978-1-59745-157-4\\_7](https://doi.org/10.1007/978-1-59745-157-4_7)
- 579 7 Kuma, A. *et al.* The role of autophagy during the early neonatal starvation period. *Nature* **432**, 1032-1036 (2004). <https://doi.org/10.1038/nature03029>
- 580 8 Yang, Y. *et al.* Autophagy in PDGFRalpha+ mesenchymal cells is essential for intestinal  
583 stem cell survival. *Proc Natl Acad Sci U S A* **119**, e2202016119 (2022).  
<https://doi.org/10.1073/pnas.2202016119>
- 581 9 Yoshii, S. R. *et al.* Systemic Analysis of Atg5-Null Mice Rescued from Neonatal  
586 Lethality by Transgenic ATG5 Expression in Neurons. *Dev Cell* **39**, 116-130 (2016).  
<https://doi.org/10.1016/j.devcel.2016.09.001>
- 582 10 Poillet-Perez, L. *et al.* Autophagy promotes growth of tumors with high mutational  
589 burden by inhibiting a T-cell immune response. *Nat Cancer* **1**, 923-934 (2020).  
<https://doi.org/10.1038/s43018-020-00110-7>
- 583 11 Poillet-Perez, L. *et al.* Autophagy maintains tumour growth through circulating arginine. *Nature* **563**, 569-573 (2018). <https://doi.org/10.1038/s41586-018-0697-7>
- 584 12 Ueno, T. & Komatsu, M. Autophagy in the liver: functions in health and disease. *Nat Rev Gastroenterol Hepatol* **14**, 170-184 (2017). <https://doi.org/10.1038/nrgastro.2016.185>
- 585 13 Komatsu, M. *et al.* Loss of autophagy in the central nervous system causes  
586 neurodegeneration in mice. *Nature* **441**, 880-884 (2006).  
<https://doi.org/10.1038/nature04723>
- 587 14 Hara, T. *et al.* Suppression of basal autophagy in neural cells causes neurodegenerative  
589 disease in mice. *Nature* **441**, 885-889 (2006). <https://doi.org/10.1038/nature04724>
- 588 15 Guo, F., Liu, X., Cai, H. & Le, W. Autophagy in neurodegenerative diseases:  
589 pathogenesis and therapy. *Brain Pathol* **28**, 3-13 (2018).  
<https://doi.org/10.1111/bpa.12545>
- 589 16 Singh, R. *et al.* Autophagy regulates lipid metabolism. *Nature* **458**, 1131-1135 (2009).  
<https://doi.org/10.1038/nature07976>
- 590 17 Yule, M. S., Brown, L. R., Skipworth, R. J. E. & Laird, B. J. A. Central neural  
591 mechanisms of cancer cachexia. *Curr Opin Support Palliat Care* **18**, 138-144 (2024).  
<https://doi.org/10.1097/SPC.0000000000000707>
- 591 18 Olson, B., Diba, P., Korzun, T. & Marks, D. L. Neural Mechanisms of Cancer Cachexia.  
592 *Cancers (Basel)* **13** (2021). <https://doi.org/10.3390/cancers13163990>

- 610 19 Cimino, I., Coll, A. P. & Yeo, G. S. H. GDF15 and energy balance: homing in on a  
611 mechanism. *Nat Med* **23**, 1119-1120 (2017). <https://doi.org/10.1038/nm.4414>
- 612 20 Hsu, J. Y. *et al.* Non-homeostatic body weight regulation through a brainstem-restricted  
613 receptor for GDF15. *Nature* **550**, 255-259 (2017). <https://doi.org/10.1038/nature24042>
- 614 21 Mulligan, S. E. *et al.* GFRAL is the receptor for GDF15 and the ligand promotes weight  
615 loss in mice and nonhuman primates. *Nat Med* **23**, 1150-1157 (2017).  
<https://doi.org/10.1038/nm.4392>
- 616 22 Emmerson, P. J. *et al.* The metabolic effects of GDF15 are mediated by the orphan  
617 receptor GFRAL. *Nat Med* **23**, 1215-1219 (2017). <https://doi.org/10.1038/nm.4393>
- 618 23 Lu, B. *et al.* Abnormalities in monocyte recruitment and cytokine expression in monocyte  
619 chemoattractant protein 1-deficient mice. *J Exp Med* **187**, 601-608 (1998).  
<https://doi.org/10.1084/jem.187.4.601>
- 620 24 Wang, D. *et al.* GDF15 promotes weight loss by enhancing energy expenditure in muscle.  
621 *Nature* **619**, 143-150 (2023). <https://doi.org/10.1038/s41586-023-06249-4>
- 622 25 Zhang, X. *et al.* CXCL10 plays a key role as an inflammatory mediator and a non-  
623 invasive biomarker of non-alcoholic steatohepatitis. *J Hepatol* **61**, 1365-1375 (2014).  
<https://doi.org/10.1016/j.jhep.2014.07.006>
- 624 26 Tomita, K. *et al.* CXCL10-Mediates Macrophage, but not Other Innate Immune Cells-  
625 Associated Inflammation in Murine Nonalcoholic Steatohepatitis. *Sci Rep* **6**, 28786  
626 (2016). <https://doi.org/10.1038/srep28786>
- 627 27 Dufour, J. H. *et al.* IFN-gamma-inducible protein 10 (IP-10; CXCL10)-deficient mice  
628 reveal a role for IP-10 in effector T cell generation and trafficking. *J Immunol* **168**, 3195-  
629 3204 (2002). <https://doi.org/10.4049/jimmunol.168.7.3195>
- 630 28 Roca, H. *et al.* CCL2 and interleukin-6 promote survival of human CD11b+ peripheral  
631 blood mononuclear cells and induce M2-type macrophage polarization. *J Biol Chem* **284**,  
632 34342-34354 (2009). <https://doi.org/10.1074/jbc.M109.042671>
- 633 29 Luciano-Mateo, F. *et al.* Chemokine C-C motif ligand 2 overexpression drives tissue-  
634 specific metabolic responses in the liver and muscle of mice. *Sci Rep* **10**, 11954 (2020).  
<https://doi.org/10.1038/s41598-020-68769-7>
- 635 30 Sell, H., Dietze-Schroeder, D., Kaiser, U. & Eckel, J. Monocyte chemotactic protein-1 is  
636 a potential player in the negative cross-talk between adipose tissue and skeletal muscle.  
*Endocrinology* **147**, 2458-2467 (2006). <https://doi.org/10.1210/en.2005-0969>
- 637 31 Sasaki, Y. *et al.* NOX4 Regulates CCR2 and CCL2 mRNA Stability in Alcoholic Liver  
638 Disease. *Sci Rep* **7**, 46144 (2017). <https://doi.org/10.1038/srep46144>
- 639 32 Bose, S. & Cho, J. Role of chemokine CCL2 and its receptor CCR2 in neurodegenerative  
640 diseases. *Arch Pharm Res* **36**, 1039-1050 (2013). <https://doi.org/10.1007/s12272-013-0161-z>
- 641 33 Haringman, J. J. *et al.* A randomized controlled trial with an anti-CCL2 (anti-monocyte  
642 chemotactic protein 1) monoclonal antibody in patients with rheumatoid arthritis.  
*Arthritis Rheum* **54**, 2387-2392 (2006). <https://doi.org/10.1002/art.21975>
- 643 34 Tsui, P. *et al.* Generation, characterization and biological activity of CCL2 (MCP-1/JE)  
644 and CCL12 (MCP-5) specific antibodies. *Hum Antibodies* **16**, 117-125 (2007).
- 645 35 Loberg, R. D. *et al.* Targeting CCL2 with systemic delivery of neutralizing antibodies  
646 induces prostate cancer tumor regression in vivo. *Cancer Res* **67**, 9417-9424 (2007).  
<https://doi.org/10.1158/0008-5472.CAN-07-1286>

- 655 36 Pienta, K. J. *et al.* Phase 2 study of carlumab (CNTO 888), a human monoclonal antibody  
656 against CC-chemokine ligand 2 (CCL2), in metastatic castration-resistant prostate cancer.  
657 *Invest New Drugs* **31**, 760-768 (2013). <https://doi.org/10.1007/s10637-012-9869-8>
- 658 37 Fleming, A. *et al.* The different autophagy degradation pathways and neurodegeneration.  
659 *Neuron* **110**, 935-966 (2022). <https://doi.org/10.1016/j.neuron.2022.01.017>
- 660 38 Le Thuc, O. *et al.* Central CCL2 signaling onto MCH neurons mediates metabolic and  
661 behavioral adaptation to inflammation. *EMBO Rep* **17**, 1738-1752 (2016).  
<https://doi.org/10.15252/embr.201541499>
- 663 39 Steuernagel, L. *et al.* HypoMap-a unified single-cell gene expression atlas of the murine  
664 hypothalamus. *Nat Metab* **4**, 1402-1419 (2022). <https://doi.org/10.1038/s42255-022-00657-y>
- 666 40 Ewart-Toland, A., Mounzih, K., Qiu, J. & Chehab, F. F. Effect of the genetic background  
667 on the reproduction of leptin-deficient obese mice. *Endocrinology* **140**, 732-738 (1999).  
<https://doi.org/10.1210/endo.140.2.6470>
- 669 41 Fantuzzi, G. & Faggioni, R. Leptin in the regulation of immunity, inflammation, and  
670 hematopoiesis. *J Leukoc Biol* **68**, 437-446 (2000).
- 671 42 Tian, D. S. *et al.* Chemokine CCL2-CCR2 Signaling Induces Neuronal Cell Death via  
672 STAT3 Activation and IL-1beta Production after Status Epilepticus. *J Neurosci* **37**, 7878-  
673 7892 (2017). <https://doi.org/10.1523/JNEUROSCI.0315-17.2017>
- 674 43 Joly-Amado, A. *et al.* CCL2 Overexpression in the Brain Promotes Glial Activation and  
675 Accelerates Tau Pathology in a Mouse Model of Tauopathy. *Front Immunol* **11**, 997  
676 (2020). <https://doi.org/10.3389/fimmu.2020.00997>
- 677 44 Alissa, N. *et al.* CCL2 signaling promotes skeletal muscle wasting in non-tumor and  
678 breast tumor models. *Dis Model Mech* **17** (2024). <https://doi.org/10.1242/dmm.050398>
- 679 45 Liu, M. *et al.* The crosstalk between macrophages and cancer cells potentiates pancreatic  
680 cancer cachexia. *Cancer Cell* **42**, 885-903 e884 (2024).  
<https://doi.org/10.1016/j.ccr.2024.03.009>
- 682 46 Mul, J. D. *et al.* Chronic loss of melanin-concentrating hormone affects motivational  
683 aspects of feeding in the rat. *PLoS One* **6**, e19600 (2011).  
<https://doi.org/10.1371/journal.pone.0019600>
- 685 47 Mul, J. D. *et al.* Pmch expression during early development is critical for normal energy  
686 homeostasis. *Am J Physiol Endocrinol Metab* **298**, E477-488 (2010).  
<https://doi.org/10.1152/ajpendo.00154.2009>
- 688 48 Ferrer, M. *et al.* Cachexia: A systemic consequence of progressive, unresolved disease.  
689 *Cell* **186**, 1824-1845 (2023). <https://doi.org/10.1016/j.cell.2023.03.028>
- 690 49 Plata-Salaman, C. R. Central nervous system mechanisms contributing to the cachexia-  
691 anorexia syndrome. *Nutrition* **16**, 1009-1012 (2000). [https://doi.org/10.1016/s0899-9007\(00\)00413-5](https://doi.org/10.1016/s0899-9007(00)00413-5)
- 693 50 Ichimiya, T. *et al.* Autophagy and Autophagy-Related Diseases: A Review. *Int J Mol Sci*  
694 **21** (2020). <https://doi.org/10.3390/ijms21238974>
- 695 51 Ruzankina, Y. *et al.* Deletion of the developmentally essential gene ATR in adult mice  
696 leads to age-related phenotypes and stem cell loss. *Cell Stem Cell* **1**, 113-126 (2007).  
<https://doi.org/10.1016/j.stem.2007.03.002>
- 698 52 Ingalls, A. M., Dickie, M. M. & Snell, G. D. Obese, a new mutation in the house mouse.  
699 *Obes Res* **4**, 101 (1996). <https://doi.org/10.1002/j.1550-8528.1996.tb00519.x>

- 700 53 Mina, A. I. *et al.* CalR: A Web-Based Analysis Tool for Indirect Calorimetry  
701 Experiments. *Cell Metab* **28**, 656-666 e651 (2018).  
<https://doi.org/10.1016/j.cmet.2018.06.019>
- 703 54 Kim, D., Langmead, B. & Salzberg, S. L. HISAT: a fast spliced aligner with low memory  
704 requirements. *Nat Methods* **12**, 357-360 (2015). <https://doi.org/10.1038/nmeth.3317>
- 705 55 Mudge, J. M. & Harrow, J. Creating reference gene annotation for the mouse C57BL6/J  
706 genome assembly. *Mamm Genome* **26**, 366-378 (2015). <https://doi.org/10.1007/s00335-015-9583-x>
- 708 56 Liao, Y., Smyth, G. K. & Shi, W. The Subread aligner: fast, accurate and scalable read  
709 mapping by seed-and-vote. *Nucleic Acids Res* **41**, e108 (2013).  
<https://doi.org/10.1093/nar/gkt214>
- 711 57 Love, M. I., Huber, W. & Anders, S. Moderated estimation of fold change and dispersion  
712 for RNA-seq data with DESeq2. *Genome Biol* **15**, 550 (2014).  
<https://doi.org/10.1186/s13059-014-0550-8>
- 714 58 Wolf, F. A., Angerer, P. & Theis, F. J. SCANPY: large-scale single-cell gene expression  
715 data analysis. *Genome Biol* **19**, 15 (2018). <https://doi.org/10.1186/s13059-017-1382-0>
- 716 59 Khayati, K. *et al.* Autophagy compensates for Lkb1 loss to maintain adult mice  
717 homeostasis and survival. *eLife* **9** (2020). <https://doi.org/10.7554/eLife.62377>
- 718 60 Su, X. *et al.* In-Source CID Ramping and Covariant Ion Analysis of Hydrophilic  
719 Interaction Chromatography Metabolomics. *Anal Chem* **92**, 4829-4837 (2020).  
<https://doi.org/10.1021/acs.analchem.9b04181>
- 721 61 Melamud, E., Vastag, L. & Rabinowitz, J. D. Metabolomic analysis and visualization  
722 engine for LC-MS data. *Anal Chem* **82**, 9818-9826 (2010).  
<https://doi.org/10.1021/ac1021166>
- 723
- 724

725

726 **Figure 1: Systemic metabolic impairment due to loss of autophagy causes cachexia**

727 **a**, Mouse body mass post TAM injection in *Atg7<sup>+/+</sup>* mice ( $n = 5$ ) and *Atg7<sup>Δ/Δ</sup>* mice ( $n = 7$ ) **b,c** Lean  
728 mass in grams and fat mass percentage loss post TAM injection in *Atg7<sup>+/+</sup>* mice ( $n = 5$ ) and *Atg7<sup>Δ/Δ</sup>*  
729 mice ( $n = 5$ ). Body composition was measured by EchoMRI. All data are mean  $\pm$  s.e.m. \* $P < 0.05$ ,  
730 \*\* $P < 0.01$ , \*\*\* $P < 0.001$ , \*\*\*\* $P < 0.0001$  using a two-sided Student's *t*-test. **d**, Body mass  
731 subtracted by liver weight at 10 weeks post TAM in *Atg7<sup>+/+</sup>* mice ( $n = 4$ ) and *Atg7<sup>Δ/Δ</sup>* mice ( $n = 5$ )  
732 **e-j**, Mice were housed in Promethion metabolic cages ( $n = 4-21/\text{group}$ ). Shaded regions represent  
733 the dark cycle from 19:00 pm to 7:00 am. **e**, daily ambulatory activity at 2- and 8- weeks post TAM  
734 . **f**, total wheel running at 2 weeks post TAM. **g**, Hourly mean of RER at 2- and 8- weeks post  
735 TAM. **h**, Overall hourly means of RER at 2- and 8- weeks post TAM. **i**, Total energy expenditure.  
736 **j**, daily food intake. **k**, Serum (GDF15 ELISA) and cytokine and chemokine profiling (CXCL10  
737 and CCL2) ( $n = 5-11/\text{group}$ ) of *Atg7<sup>+/+</sup>* and *Atg7<sup>Δ/Δ</sup>* mice.

738

739 **Figure 2: Induction of CCL2 contributes to lethality during autophagy deficiency**

740 **a**, Kaplan-Meier survival curve of *Atg7<sup>+/+</sup>*, *Atg7<sup>Δ/Δ</sup>*, *Ccl2<sup>-/-</sup>*, and *Ccl2<sup>-/-</sup>;Atg7<sup>Δ/Δ</sup>* mice. **b**,  
741 Representative images of *Atg7<sup>+/+</sup>*, *Atg7<sup>Δ/Δ</sup>*, *Ccl2<sup>-/-</sup>*, and *Ccl2<sup>-/-</sup>;Atg7<sup>Δ/Δ</sup>* mice at 8- and 42- weeks  
742 post TAM injection. **c**, Kaplan-Meier 24 hours fasting survival curve of *Atg7<sup>+/+</sup>*, *Atg7<sup>Δ/Δ</sup>*, *Ccl2<sup>-/-</sup>*,  
743 and *Ccl2<sup>-/-</sup>;Atg7<sup>Δ/Δ</sup>* mice 10 days post-TAM. **d**, Blood glucose and plasma insulin measurements  
744 collected at 16-hour post fast. **e**, Blood glucose following an intraperitoneal lactate tolerance  
745 test. Area under curve calculated from individual blood glucose traces. (\*)  $P < 0.05$ ; (\*\*\*)  $P <$   
746 0.001; (\*\*\*\*)  $P < 0.0001$ ; (n.s.) not significant (unpaired *t*-test). **f-i**, Statistical analysis of the  
747 main altered metabolites enrichment in plasma of *Atg7<sup>+/+</sup>*, *Atg7<sup>Δ/Δ</sup>*, *Ccl2<sup>-/-</sup>*,  
748 and *Ccl2<sup>-/-</sup>;Atg7<sup>Δ/Δ</sup>* mice after *in vivo* <sup>13</sup>C lactate tracing at 2 weeks post deletion. **f**, Lactate  
749 enrichment **h**, glucose enrichment **i**, ratio glucose/lactate enrichment. For all graphs the  $P$  values  
750 were determined using one-way ANOVA.  $P$  values are indicated as  $\leq 0.05^*$ ,  $\leq 0.01^{**}$ ,  $\leq 0.001^{***}$ ,  
751 and  $\leq 0.0001^{****}$ .

752

753 **Figure 3: Metabolic Phenotyping shows Loss of CCL2 impacts body composition and food  
754 intake.**

755 **a**, Mouse body weight post TAM injection in *Atg7<sup>+/+</sup>*, *Atg7<sup>Δ/Δ</sup>* mice, *Ccl2<sup>-/-</sup>* mice,  
756 and *Ccl2<sup>-/-</sup>;Atg7<sup>Δ/Δ</sup>* mice over 365 days. **b,c** Lean mass and fat mass over 42 weeks post TAM  
757 injection in *Atg7<sup>+/+</sup>*, *Atg7<sup>Δ/Δ</sup>* mice, *Ccl2<sup>-/-</sup>* mice, and *Ccl2<sup>-/-</sup>;Atg7<sup>Δ/Δ</sup>*. Body composition was  
758 measured by EchoMRI. All data are mean  $\pm$  s.e.m. \* $P < 0.05$ , \*\* $P < 0.01$ , \*\*\* $P < 0.01$ ,  
759 \*\*\*\* $P < 0.0001$  using a two-sided Student's *t*-test. **d-h**, Mice were housed in Promethion  
760 metabolic cages ( $n = 4-11/\text{group}$ ). Shaded regions represent the dark cycle from 19:00 pm to 7:00  
761 am. **d**, daily ambulatory activity at 2 weeks post TAM. **e**, Hourly mean of RER at 2- and 8- weeks post  
762 TAM. **f**, Overall hourly means of RER at 2- and 8- weeks post TAM. **g**, Total energy expenditure.  
763 **h**, daily food intake.

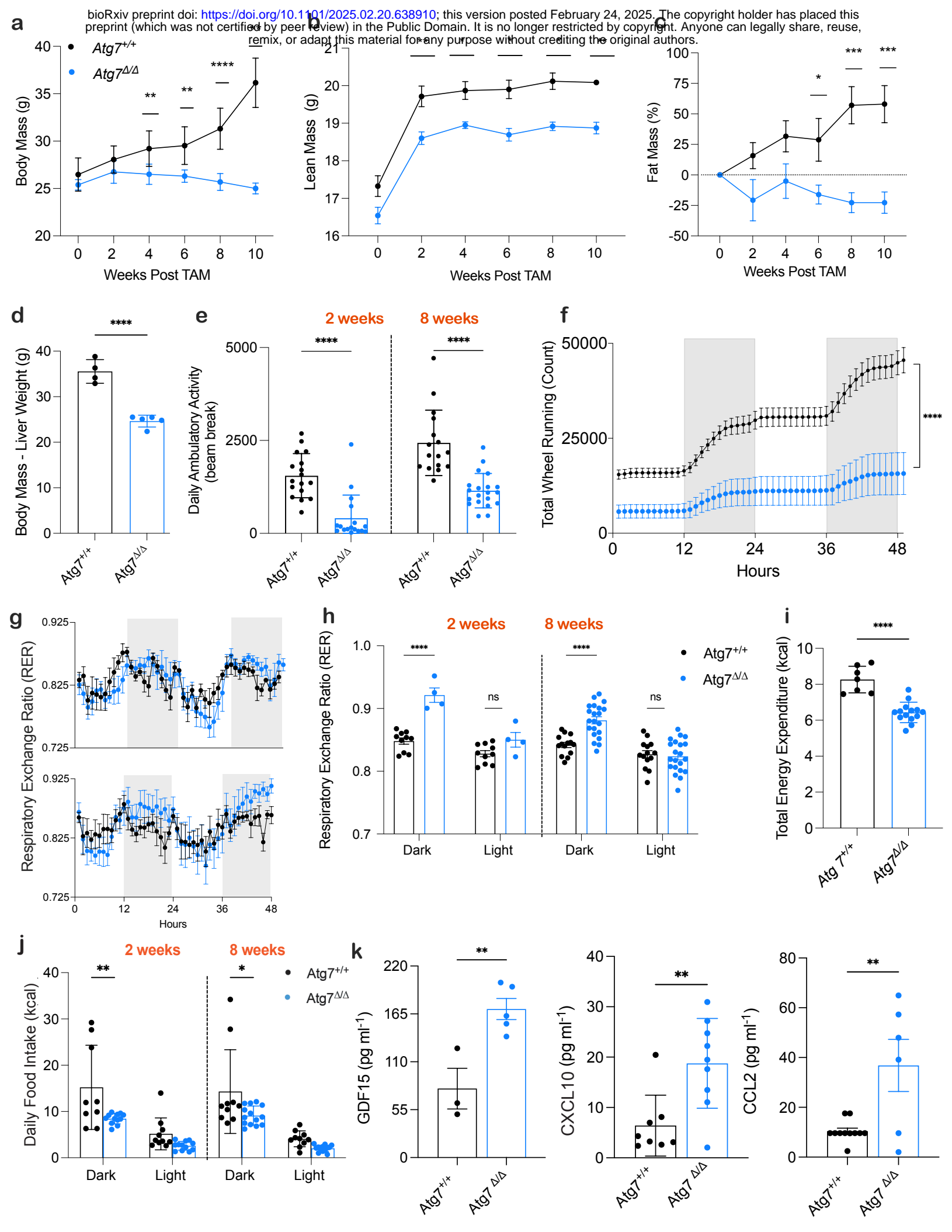
764

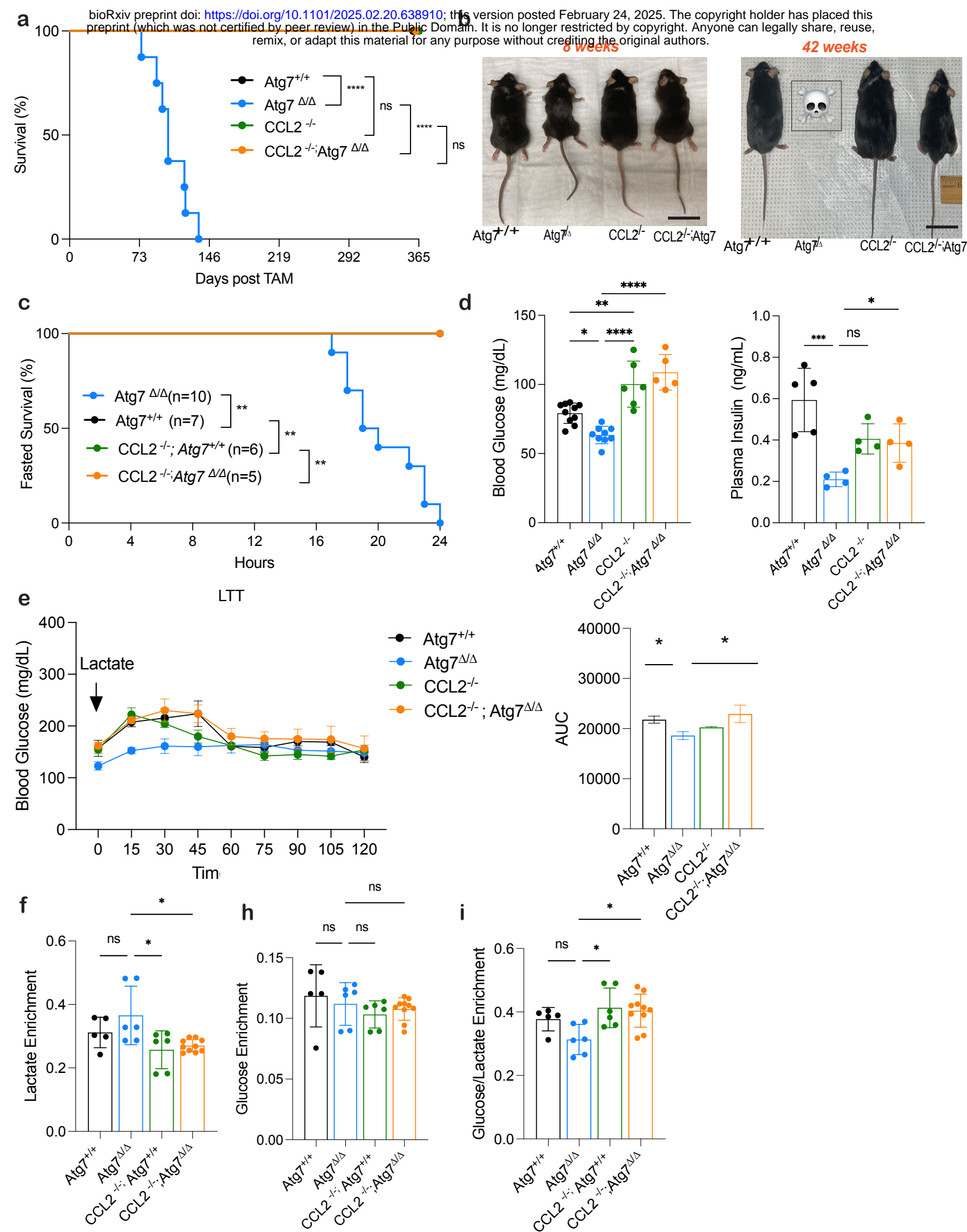
765 **Figure 4: Diversity and proportion of cell types in the scRNA-seq of the hypothalamus from  
766 wild-type and *Ccl2<sup>-/-</sup>* mice with and without deletion of *Atg7*.**

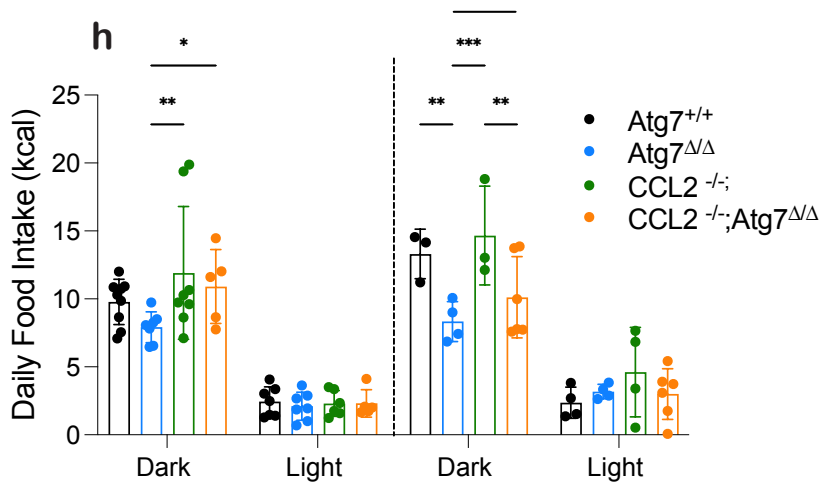
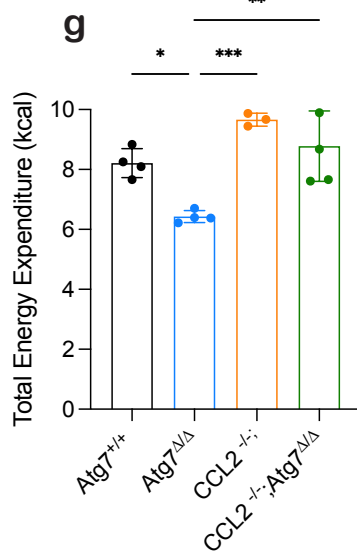
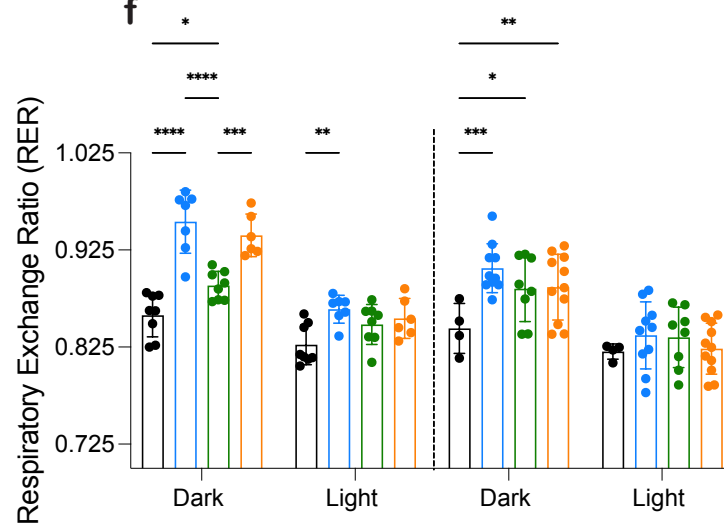
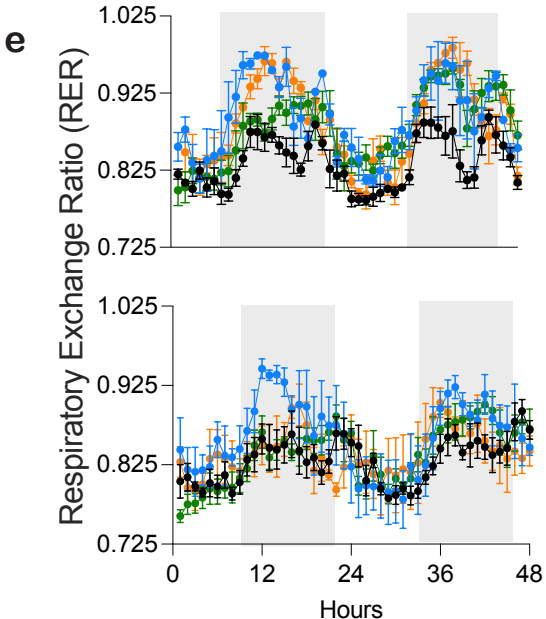
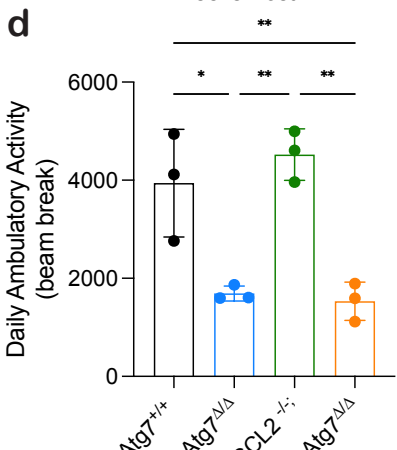
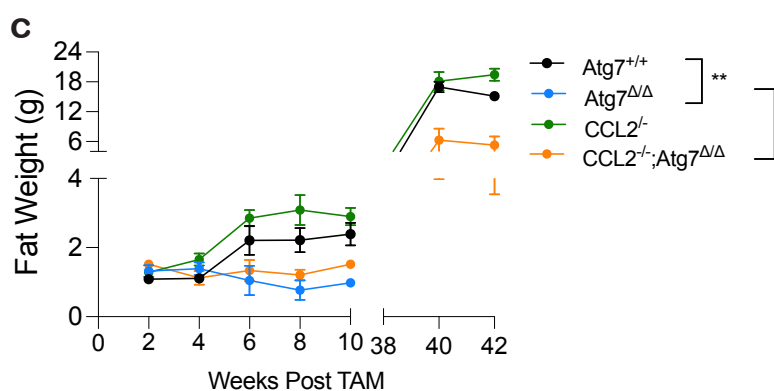
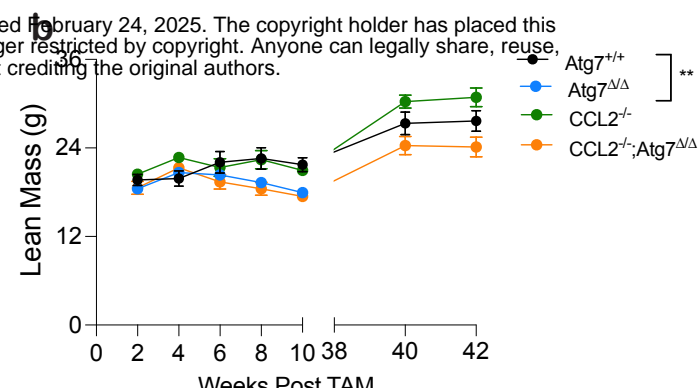
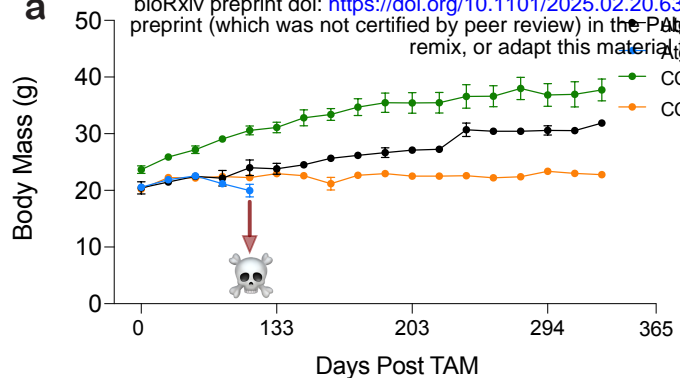
767 **a**, Uniform Manifold Approximation and Projection (UMAP) of the snRNA-seq data with cell  
768 type annotations for *Atg7<sup>Δ/Δ</sup>*, *Ccl2<sup>-/-</sup>*, and *Ccl2<sup>-/-</sup>;Atg7<sup>Δ/Δ</sup>* mice at the 8-wk time point. **b**, UMAP  
769 showing 52 clusters that were used to annotate cell types. **c**, UMAP showing the cells separately  
770 for *Atg7<sup>Δ/Δ</sup>*, *Ccl2<sup>-/-</sup>*, and *Ccl2<sup>-/-</sup>;Atg7<sup>Δ/Δ</sup>* mice. **d**, Bar plot depicting the cluster composition across

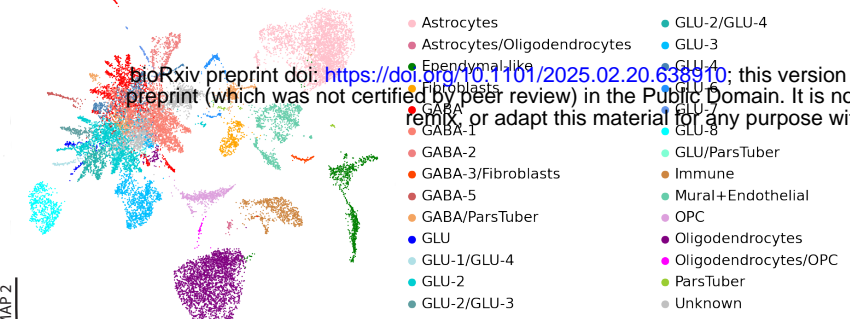
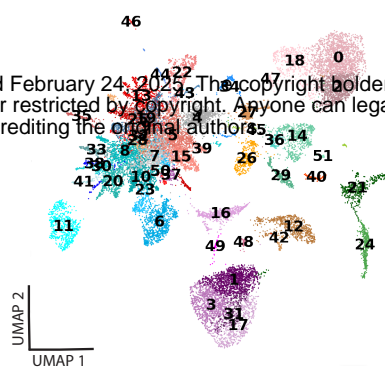
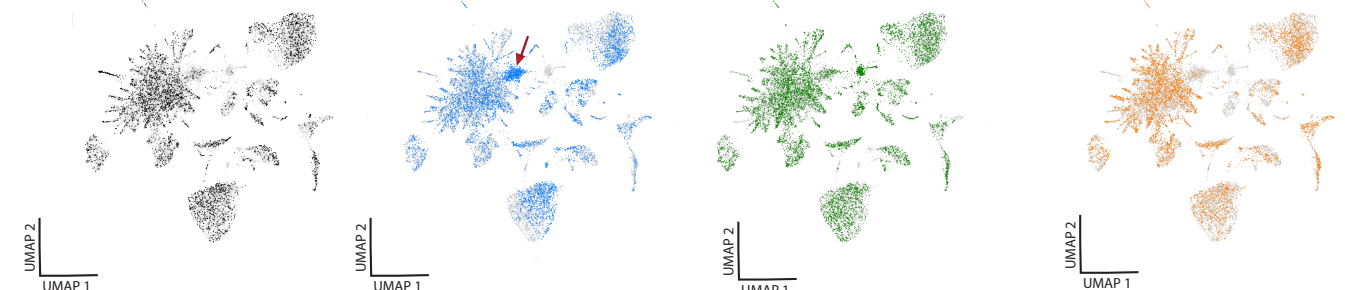
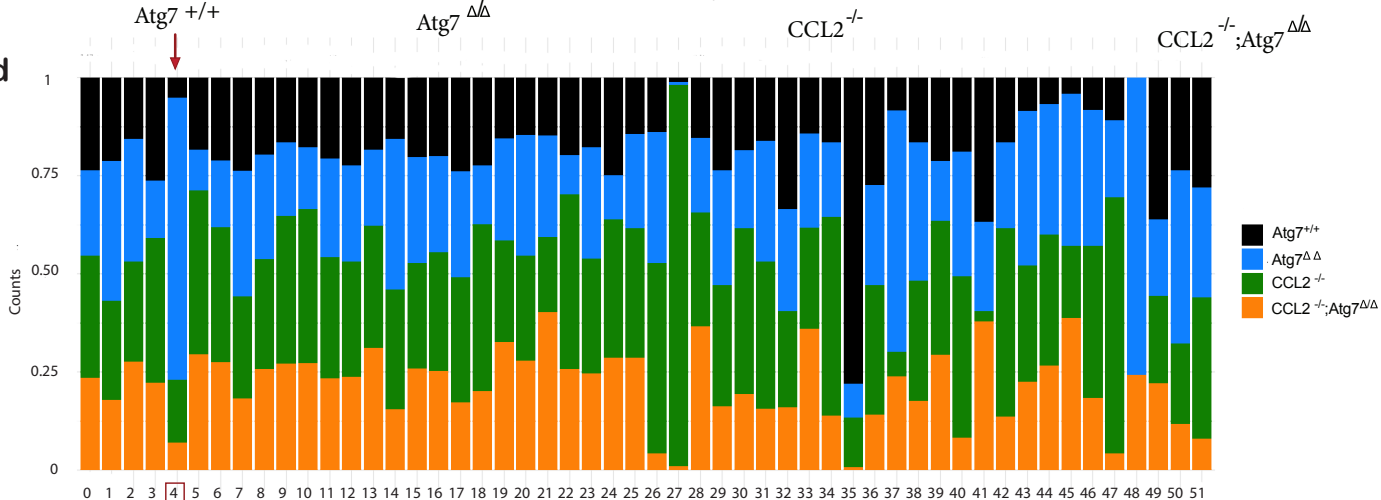
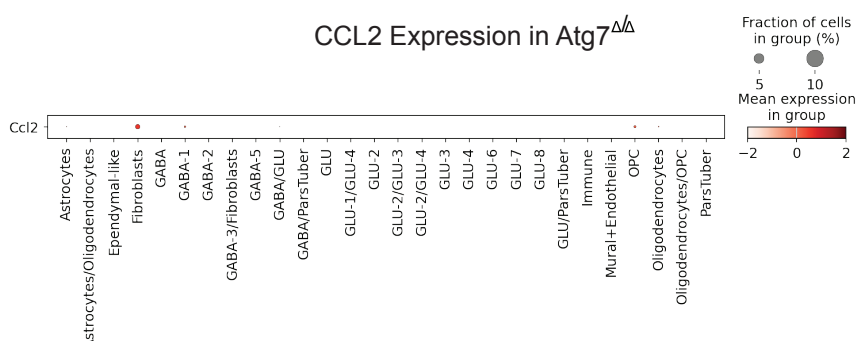
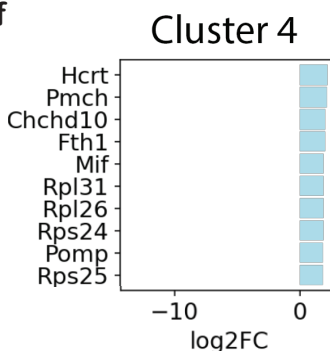
771 the different samples. **e**, Expression of CCL2 across cell types in *Atg7<sup>Δ/Δ</sup>* mice. **f**, Top 10  
772 upregulated genes in Cluster 4. **g**, Schematic of snRNA-seq results due to loss of CCL2.  
773

774 **Figure 5: ob/ob rescues lethality and weight loss induced by autophagy deficiency.**  
775 **a**, Kaplan-Meier survival curve of *Atg7<sup>+/+</sup>*, *Atg7<sup>Δ/Δ</sup>*, *ob/ob*, and *ob/ob;Atg7<sup>Δ/Δ</sup>* mice. **b**,  
776 Representative images of *Atg7<sup>+/+</sup>*, *Atg7<sup>Δ/Δ</sup>* mice, *ob/ob* mice, and *ob/ob;Atg7<sup>Δ/Δ</sup>* mice at 8- and 42-  
777 weeks post TAM injection. **c**, Mouse body weight post TAM injection in  
778 *Atg7<sup>+/+</sup>*, *Atg7<sup>Δ/Δ</sup>* mice, *ob/ob* mice, and *ob/ob;Atg7<sup>Δ/Δ</sup>* mice. **d-e**, Fat mass and lean mass loss post  
779 TAM injection in mice. Body composition was measured by EchoMRI. All data are mean ± s.e.m.  
780 \* $P < 0.05$ , \*\* $P < 0.01$ , \*\*\* $P < 0.01$ , \*\*\*\* $P < 0.0001$  using a two-sided Student's *t*-test. **f**, Serum  
781 CCL2 ELISA. **g**, Kaplan-Meier 24 hours fasting survival curve of *Atg7<sup>+/+</sup>*, *Atg7<sup>Δ/Δ</sup>*, *ob/ob*,  
782 and *ob/ob;Atg7<sup>Δ/Δ</sup>* mice 10 days post-TAM. Blood glucose collected at 16-hour post fast. **h**, daily  
783 food intake. **k**, Proposed graphical summary of lethality in autophagy deficient mice.  
784  
785  
786







**a****b****c****d****e****f****g**